Front. Earth Sci. 2024, 18(2): 296–311
https://doi.org/10.1007/s11707-022-1057-3

RESEARCH ARTICLE

# Geochemical characteristics, generation, and evolution mechanism of coalbed methane in the south-western Ordos Basin, China

**Yabing LIN (✉)[1,2,3], Yong QIN[2], Dongmin MA[1,3], Shengquan WANG[1,3]**

1 College of Geology and Environment, Xi'an University of Science and Technology, Xi'an 710054, China
2 Key Laboratory of Coalbed Methane Resource and Reservoir Formation Process (the Ministry of Education), China University of Mining and Technology, Xuzhou 221008, China
3 Shaanxi Provincial Key Laboratory of Geological Support for Coal Green Exploitation, Xi'an 710054, China



**Abstract** The south-western Ordos Basin is rich in low-middle rank coalbed methane (CBM) resources; while the geochemical characteristics and genetic mechanism of CBM are not clear. Herein, according to geological and geochemical test data from gas and coal seam water from CBM wells in Bingchang, Jiaoxun, Huangling, Yonglong, and Longdong minging areas, we systematically studied the geochemical characteristics, generation, and evolution mechanism of CBM in Jurassic Yan'an Formation in the south-western Ordos Basin. The results show that the $CH_4$ content of whole gas is in the range of 42.01%–94.72%. The distribution ranges of the $\delta^{13}C$-$CH_4$ value is −87.2‰ to −32.5‰, indicating diverse sources of thermogenic gas and biogenic gas. The microbial methane is mainly generated by a $CO_2$ reduction pathway, with certain methyl-type fermentation spots. The $\delta^{13}C$-$CH_4$ has a positive correlation with burial depth, indicating the obvious fractionation of CBM. The relationship between the genetic types and burial depth of the CBM reservoir indicates that the favorable depth of secondary biogenic gas is less than 660 m. The Late Cretaceous Yanshanian Movement led to the uplift of the Ordos Basin, and a large amount of thermogenic gas escaped from the edge of the basin. Since the Paleogene Period, the coal reservoir in the basin margin has received recharge from atmospheric precipitation, which is favorable for the formation of secondary biogenic methane. The deep area, generally under 1000 m, mainly contains residual thermogenic gas. The intermediate transition zone is mixed gas. Constrained by the tectonic background, the genetic types of CBM in different mining areas are controlled by the coupling of burial depth, coal rank, and hydrogeological conditions. The Binchang mining area contains biogenic gas, and the development of CBM has achieved initial success, indicating that similar blocks with biogenic gas formation conditions is key to the efficient development of CBM. The research results provide a scientific basis for searching for favorable exploration areas of CBM in the south-western Ordos Basin.

**Keywords** coalbed methane, stable isotopes, geochemistry, generation and evolution mechanism, Ordos Basin

## 1 Introduction

The development of coalbed methane (CBM) can help to improve China's energy structure of "rich coal, poor oil and little gas" (Qin et al., 2018; Li et al., 2022a). Research on the isotopic composition and genesis of CBM is conducive to deepen the understanding of the accumulation mechanism of CBM (Moore, 2012; Xin et al., 2022). The CBM geology resources are as much as 777.48 × $10^8$ $m^3$ in the south-western Ordos Basin, with the characteristics of large coal seam thickness and high permeability (Xu et al., 2012; Lin, 2021). Recently, the development of CBM has achieved remarkable progresses in the Binchang, Jiaoping, and Longdong mining areas (Tao et al., 2019; Lin, 2021). In the Binchang mining area, the gas production of the DFS-133 vertical well has exceeded 3000 $m^3$/d, and the gas production of the DFS-C02 horizontal well has exceeded 30000 $m^3$/d (Lin et al., 2020). Currently, the commercial development of CBM has been realized in the Binchang mining area, which is also the first commercial development block of low-rank CBM in Jurassic in north-west China. However, the gas content in the south-

Received October 24, 2022; accepted December 21, 2022

E-mail: lybcbm@126.com

western Ordos Basin is generally low and the regional differences are large, and the mechanism of enrichment and accumulation is still unclear. Furthermore, there are also prominent problems in the area, such as the productivity of adjacent wells varies greatly and the low average gas production of a single well. Research on CBM geochemistry is helpful in improving the understanding of the formation and preservation conditions of CBM, and further provides theoretical basis for the layout and adjustment of CBM development plans in the study area.

Based on different genetic mechanisms, the methane is divided into three categories, i.e., biogenic, thermogenic, and mixed CBM (Schoell, 1980). Different CBM types are usually identified by common index such as $\delta^{13}C\text{-}CH_4$, $\delta D\text{-}CH_4$, $\delta^{13}C\text{-}CO_2$, $C_1/(C_2 + C_3)$ (drying coefficient), and CDMI (carbon dioxide–methane index) (Smith and Pallasser, 1996; Conrad, 2005; Ni et al., 2013; Bao et al., 2020). The global statistics of the CBM isotopic value show that the $\delta^{13}C\text{-}CH_4$ variation range is generally −88‰ to −17‰, $\delta D\text{-}CH_4$ is −415‰ to −75‰, and $\delta^{13}C\text{-}CO_2$ is −54‰ to +26‰ (Kotarba and Rice, 2001; Milkov and Etiope, 2018). The typical $\delta^{13}C\text{-}CH_4$ value of thermogenic methane is usually from −20‰ to −40‰, while the $\delta^{13}C\text{-}CH_4$ value of biogenic gas from microbial acetate fermentation and $CO_2$ reduction is usually lower than −55 ‰, even as low as −60 ‰ (Ni et al., 2013; Milkov et al., 2020). Values of $\delta^{13}C\text{-}CH_4$ and $\delta D\text{-}CH_4$ increase with the increased degree of coalification ($R_o$), and logarithmic equations of $\delta^{13}C\text{-}CH_4$ and $R_o$ have been established for several regions (Qin et al., 2000; Meng et al., 2017). The hydrogen isotope composition of methane can reflect the sedimentary environment of the parent material. The $\delta D\text{-}CH_4$ value of biogenic methane generated in the marine environment is from −170‰ to −250 ‰, and the $\delta D\text{-}CH_4$ value of biogenic methane generated in the freshwater environment of the land is from −250‰ to −400‰ (Whiticar et al., 1986; Whiticar, 1996; Gutsalo, 2008). Simultaneously, the $\delta D\text{-}CH_4$ interval values of CBM from different genetic types have obvious differences (Whiticar, 1999).

The gas contents of coal reservoirs are affected by geological structure, burial depth, and ground hydrodynamic conditions, which in turn affect the carbon isotope distribution of CBM (Chen et al., 2020; Li et al., 2022b). The type of kerogen, maturity of organic matter, desorption-diffusion-migration effect, the mixing of secondary biogenic gas (SBG), and the isotope exchange reaction between $CO_2$ and $CH_4$ are all important factors affecting the carbon isotope composition and changes of CBM (Ju et al., 2014). There is a phenomenon of $\delta^{13}C\text{-}CH_4$ fractionation in the CBM desorption-diffusion-migration process (Strąpoć et al., 2006), and the fractionation mechanisms include SBG fractionation, hydrodynamic fractionation, magma contact metamorphic fractionation, and early $CO_2$ exchange fractionation (Li et al., 2014). The CBM formed in different coalification stages has different genetic mechanisms, gas composition characteristics, and isotope composition differences (Qin et al., 2000). The genetic type of high-rank CBM is mainly thermogenic gas, the middle-rank CBM is mainly mixed genetic gas, and the low-rank CBM is mainly biogenic gas (mainly secondary biogenic gas) (Dai et al., 1986; Moore, 2012; Ju et al., 2021).

Researchers have conducted preliminary discussions on the isotope signature and enrichment mechanism of CBM in parts of the south-western Ordos Basin (Xu et al., 2012; Jin and Zhang, 2014), however, there is no systematic understanding of the genetic types, generation, and evolution mechanism of CBM from regional geology. Thus, according to the data of CBM exploration wells, production wells, and previous literature in the early stage of the south-western Ordos Basin, combined with the sampling and test results of CBM and coalbed water in this work, the chemical composition and isotopic distribution characteristics of CBM in the study area were analyzed. Combined with structural evolution, thermal evolution, burial depth, and hydrogeological conditions, the geochemical mechanism causing the difference was discussed. The research results cannot only deepen the understanding of the genesis of CBM but also provide a geological basis for CBM development in the Ordos Basin.

## 2 Sample collection and experimental methods

### 2.1 Geological background

The Ordos Basin is a critical energy basin in the central part of China, with an area larger than $2.5 \times 10^5$ km$^2$ (Li et al., 2017). The south-western part of the basin is mainly composed of two structural units, that is, the Weibei uplift and the Shanbei slope (Lin et al., 2021a). The overall structural form in the study area is a gentle slope tending to NW, and the secondary structure is mainly a gentle and discontinuous fold (Fig. 1). The stratigraphic dip in the study area is generally 3°–5°, and the maximum is 12°–15°. Generally, except for the Longxian area in the west, the fault structure in the study area is not developed.

The coal-bearing strata in the study area is the Jurassic Yan'an Formation, and its sedimentary environment is dominated by meandering river sediment (Lin et al., 2021b). Lakeshore and shallow lake facies developed in the late sequence 1 and sequence 2 sedimentary periods in the Huangling mining area (Fig. 2). Yan'an Formation can be divided into five sections and contains 1–8 layers of coal seam. The coal seam in the first section is the minable coal seam, with a general thickness of 5–8 m and a maximum thickness of 43.8 m. The burial depth of the

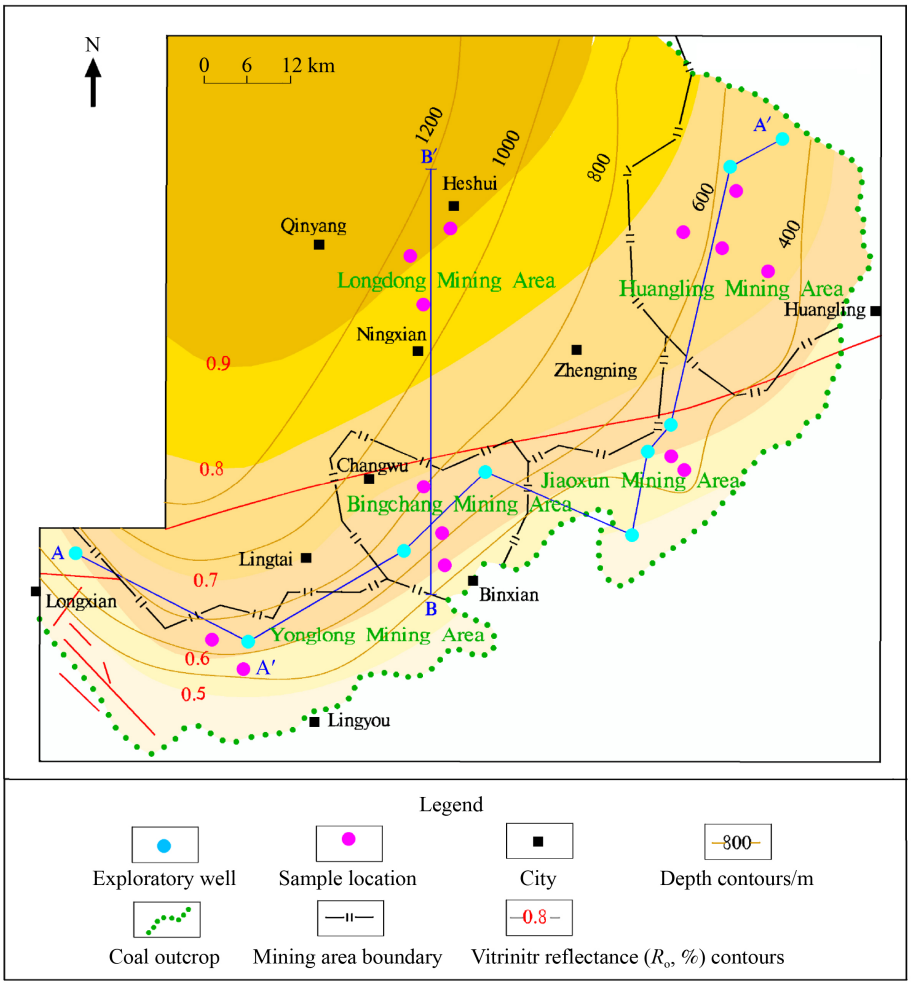


**Fig. 1** Burial depth and vitrinite reflectance contour of coal seam in the southwestern Ordos Basin; AA′ is the cross section from west to east; BB′ is the cross section from south to north.

coal reservoir is 307.4–1334.46 m, gradually increasing along the NW direction (Fig. 1). The max vitrinite reflectance ($R_{o,\,max}$) of coal is between 0.50% and 0.93%, and it gradually increases toward the north-west (Fig. 1). The coal structure is mainly primary structure, and some are cataclastic structure. The roof of the coal seams mainly comprises mudstone and carbonaceous mudstone. The floor of the coal reservoir mainly comprises mudstone, argillaceous siltstone, and sandy mudstone, and the lithology is dense and greatly thick, which makes a good capping layer and is conducive to the preservation of CBM.

## 2.2 Collection and processing of gas and water samples

Gas samples in this work were collected from CBM production wells and gas drainage hole in the coal mine. The gas was collected in a glass bottle by the drainage gas collection method, which was then sealed for gas composition and stable isotope analysis. A GC-9160 gas chromatograph was used to determine the gas compositions of CBM samples after the Chinese National Standard GB/T 13610-2014. The carbon isotope composition of $C_{1-5}$ monomers and $CO_2$ in CBM were determined by MAT253 gas isotope ratio mass spectrometer and gas chromatograph. The hydrogen isotopes of alkane components were determined by an Isoprime 100 isotope mass spectrometer. The determination process of gas stable isotopes follows the Chinese National Standard GB/T 37847-2019. Before gas isotope determination, the gas samples were first injected into the Poraplot Q column for single component separation under the drive of carrier gas (He) at a flow rate of 1.0 mL/s. The isolated $CO_2$ was directly used for $\delta^{13}C\text{-}CO_2$ analysis. The isolated hydrocarbon gases were then fed into an oxidation furnace (960°C) for $\delta^{13}C\text{-}CH_4$ analysis or into a combustion tube (1400°C) for $\delta D\text{-}CH_4$ analysis. Xing et al. (2022) gave a more detailed description of the nature gas isotope testing methods.

The coal seam water samples of the Yan'an formation are collected with a 2.5 L pure water bottle from the wellhead of the scientific well and CBM wells. To avoid the impact of fracturing fluid on the quality of coal seam water, the drainage time of CBM wells used to collect

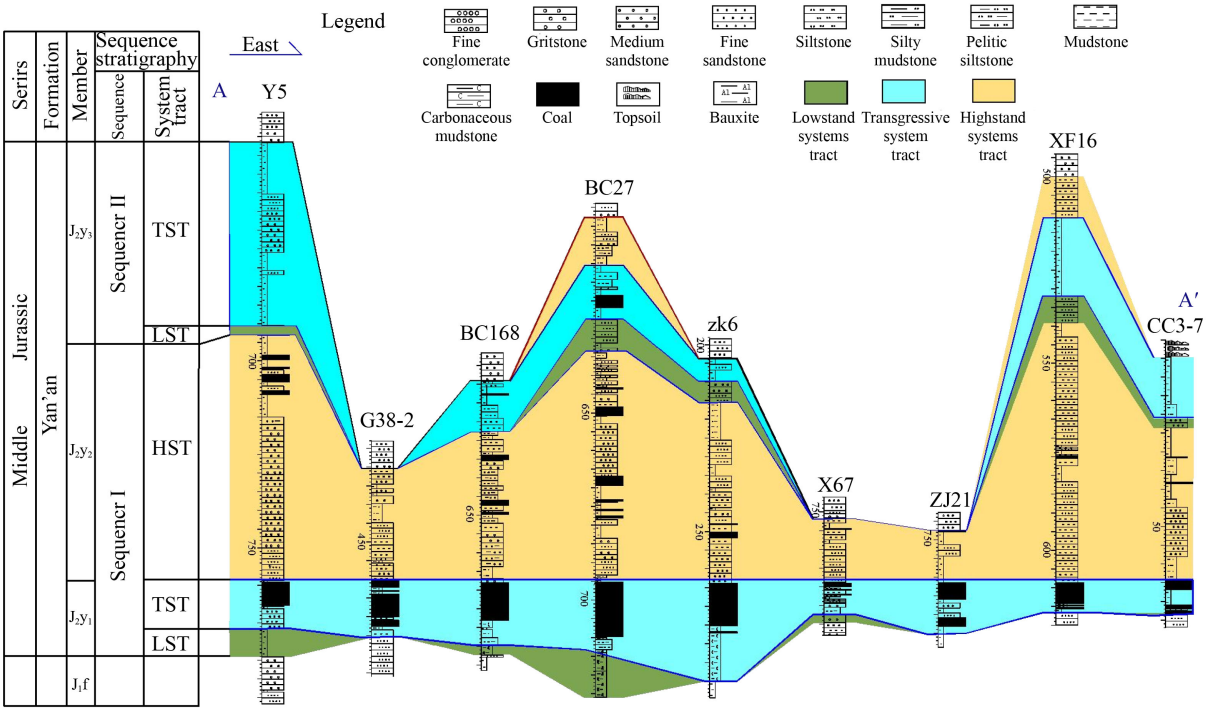


**Fig. 2** A geologic cross section of the Yan'an Formation along the A-A′ line (the section line can be found in Fig. 1).

water samples in this work is more than half a year. Before sampling, the bottle was first rinsed with the water sample three times, and then the whole bottle was fully filled with the water sample to ensure that all the air in the bottle was exhausted. Finally, the bottle cap was sealed. Water analysis was carried out based on the Geological and Mineral Industry Standard DZ/T 0064-2021, which included pH and cation and anion concentrations.

## 3 Results

### 3.1 Gas content and chemical composition of CBM

The gas content and chemical composition analysis results from the previous exploration report shown in Table 1. The gas content of coal seam on an air-dried basis varies between 0.01 and 6.31 $m^3/t$ (av. 2.08 $m^3/t$). CBM is mainly composed of methane, with a concentration of 42.01%–94.72%; next is $N_2$, with a concentration of 6.89%–45%; the $CO_2$ concentration is 0.32%–14.44%, generally less than 2%; the concentration of heavy hydrocarbon gas is 0%–6.74%, which is extremely low in the Binchang and Jiaoxun mining area. The dryness index of CBM ($C_1/(C_2 + C_3)$) is distributed from 0.91 to 1.00; except for the YC1 well sample, the others are all greater than 0.96.

Figure 3(a) shows that the gas content increases first and then decreases with the increased burial depth, and the maximum value varies between 400 and 600 m. There is a highly negative correlation between $N_2$ concentration and $CH_4$ concentration (Fig. 3(c)), which is due to CBM weathering, that let the surface air and the generated gas by chemical action enter the shallow coal seams from the surface, thus affecting the composition of CBM. Moreover, the fitting curves of heavy hydrocarbon gas concentration versus burial depth (Fig. 3(d)) and gas content versus burial depth have a mirror image relationship, indicating that the increase in heavy hydrocarbon concentration is not conducive to the increase in gas content.

Table 2 shows the stable isotope values of CBM samples. The $\delta^{13}C\text{-}CH_4$ value is distributed from −87.2‰ to −32.5‰, with an average of −57.6‰. The minimum $\delta^{13}C\text{-}CH_4$ value is significantly lower than the minimum value ( −72.3‰) in China (Ju et al., 2014) and even close to the global minimum value ( −88.0%) (Milkov and Etiope, 2018). The $\delta D\text{-}CH_4$ value varies between −268.0‰ and −205.8‰, with an average of −214.8‰. The dryness index ($C_1/(C_2 + C_3)$) in the Binchang, Yonglong, Jiaoxun, and Huangling mining areas are generally greater than 1000, while the hydrocarbon index in the Longdong area is all less than 100. Moreover, the $\delta^{13}C\text{-}CO_2$ value is distributed from −36.6‰ to −5.0‰, with an average of −20.9‰. Also, some CBM samples do not contain $CO_2$. The mean values and distribution intervals of $\delta^{13}C\text{-}CH_4$ (Fig. 4(a)) and $\delta D\text{-}CH_4$ (Fig. 4(b)) are quite different in the different mining areas (Fig. 4), indicating the different origin of CBM (discussed later).

### 3.2 Hydrochemical characteristics of Yan'an Formation

The total dissolved solid (TDS) of coalbed water in the

**Table 1** Development coal seam, gas content, and gas components of CBM in the southwestern Ordos Basin

| Mining area | Well | Coal seam | Burial depth/m | Gas component/% | | | | Dryness index | Gas content/ ($m^3 \cdot t^{-1}$) |
|---|---|---|---|---|---|---|---|---|---|
| | | | | $CH_4$ | $CO_2$ | $N_2$ | $C_{2+}$ | | |
| Yonglong | YC1 | 2 | 737 | 70.72 | 1.07 | 21.47 | 6.74 | 0.91 | 1.28 |
| | YC1 | 3 | 763 | 72.89 | 0.61 | 23.21 | 3.30 | 0.96 | 1.73 |
| | YC2 | 2 | 592 | 75.42 | 0.54 | 24.01 | 0.23 | 1.00 | 2.04 |
| | YC3 | 2 | 574 | 75.15 | 0.46 | 24.03 | 0.30 | 1.00 | 1.77 |
| | ZC01 | 2 | 307 | 76.85 | 0.56 | 20.86 | 1.74 | 0.98 | 0.15 |
| | ZC01 | 3 | 335 | 75.20 | 0.66 | 23.16 | 1.00 | 0.99 | 0.64 |
| | ZC02 | 3 | 608 | 68.96 | 1.03 | 28.68 | 1.33 | 0.98 | 0.41 |
| Binchang | DFS-1 | $4^{up}$ | 477 | n | n | n | n | n | 0.72 |
| | | 4 | 513 | 55.31 | 3.30 | 41.39 | 0 | 1.00 | 1.19 |
| | DFS-2 | $4^{up}$ | 575 | 88.33 | 0.32 | 11.34 | 0.01 | 1.00 | 2.66 |
| | | 4 | 596 | 89.80 | 0.40 | 9.79 | 0.01 | 1.00 | 3.65 |
| | DFS-3 | $4^{up}$ | 539 | 86.39 | 0.58 | 13.02 | 0.01 | 1.00 | 2.83 |
| | | 4 | 568 | 86.60 | 0.82 | 12.58 | 0 | 1.00 | 2.45 |
| | DFS-4 | $4^{up}$ | 486 | 68.52 | 4.54 | 26.94 | 0 | 1.00 | 1.79 |
| | | 4 | 499 | 69.60 | 4.65 | 25.75 | 0 | 1.00 | 1.97 |
| | DFS-152 | $4^{up}$ | 506 | 52.76 | 1.83 | 45.00 | 0 | 1.00 | 0.47 |
| | | 4 | 522 | 67.41 | 1.06 | 31.52 | 0 | 1.00 | 0.73 |
| | DFS-132 | $4^{up}$ | 459 | 74.06 | 0.92 | 25.06 | 0 | 1.00 | 0.86 |
| | | 4 | 477 | 72.49 | 1.54 | 26.00 | 0 | 1.00 | 1.34 |
| Jiaoxun | CJS-01 | 3 | 509 | 64.24 | n | n | n | n | 6.88 |
| | | $4^{-2}$ | 576 | 44.39 | n | n | n | n | 3.83 |
| | TC-01 | 3 | 507 | 91.64 | 1.47 | 6.89 | 0 | 1.00 | 4.09 |
| | | $4^{-2}$ | 541 | 85.64 | 3.34 | 10.31 | 0.71 | 0.99 | 2.93 |
| | TC-02 | 3 | 504 | 89.96 | 0.78 | 9.27 | 0 | 1.00 | 2.98 |
| | | $4^{-2}$ | 541 | 84.45 | 2.80 | 12.71 | 0 | 1.00 | 2.61 |
| Huangling | / | 2 | 350–855 | 84.62–90.13 | 0.62–1.65 | 8.53–13.25 | 0.13–1.10 | 0.99–1.00 | 0.01–6.00 |
| Longdong | / | 4 | 950–1300 | 42.01–94.72 | 1.26–14.44 | 4.00–43.52 | 0.02–3.29 | 0.96–1.00 | 0.41–6.31 |
| Max | | | 335 | 94.72 | 14.44 | 45.00 | 6.74 | 1.00 | 6.31 |
| Min | | | 1300 | 44.39 | 0.32 | 6.89 | 0 | 0.91 | 0.01 |

Note: "n" = no data; dryness index = $C_1/(C_1 + C_{2+})$.

different mining areas is distributed from 734.49 to 93898.00 mg/L, which is quite different (Table 3). The TDS from small to large are Yonglong, Jiaoxun, Huangling, Binchang, and Longdong mining areas (Fig. 5). Except the Yonglong mining area, the salinity of produced water is generally high. The produced water mainly includes three types of water quality: Na–Cl, Na–$SO_4$, and Na–$HCO_3$ (Fig. 6). Among them, Jiaoping is of Na–Cl type, Yonglong is dominated by Na-$SO_4$ and Na–Cl type; Binchang is dominated by Na–Cl and Na-$SO_4$ type; Huangling is of Na–$SO_4$ type; Longdong is dominated by the Na–Cl and Na–$HCO_3$ type. The PH value of produced water in the study area ranges from 6.00 to 8.46. Except that the water in Longdong mining area is weakly acidic water, the water in other mining areas is neutral to weak alkaline as a whole.

### 3.3 Source of CBM

The variations in the isotopic composition of CBM are related to the gas generation stage and mechanism (Whiticar, 1999; Qin et al., 2000). The isotopic value of CBM in the study area has a wide distribution range and varies greatly in the different mining areas. This indicates the complicated genesis of CBM (Fig. 4). If a single index is used, it cannot effectively distinguish the overlapping zones of different genetic types of gas (Whiticar et al., 1986; Tao et al., 2021). Hence, $\delta^{13}C$-

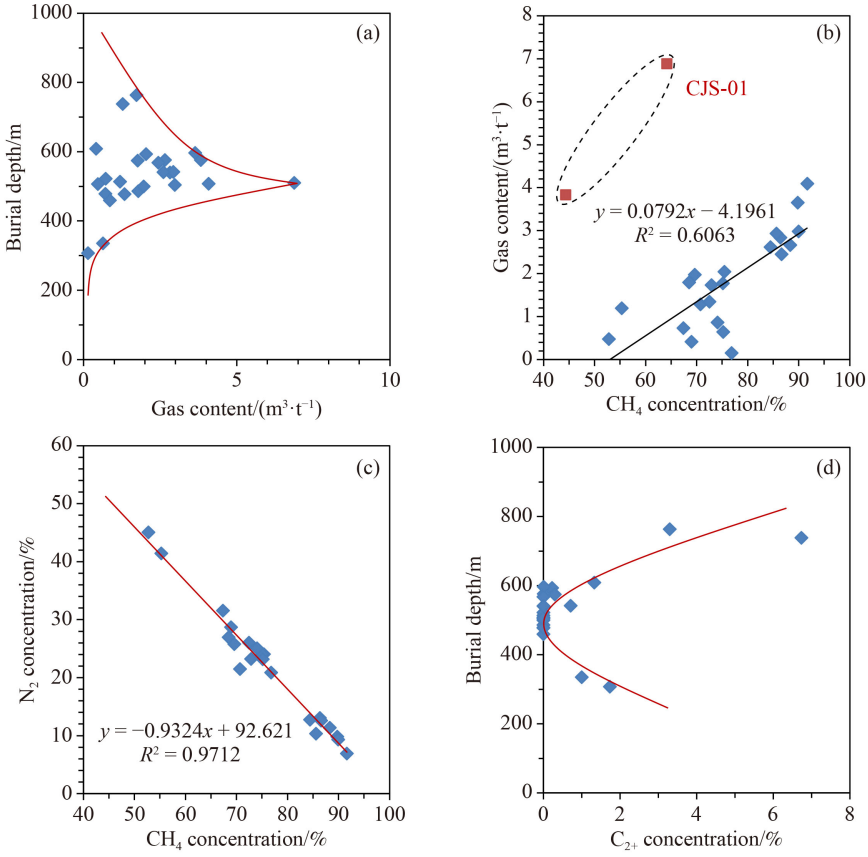


**Fig. 3** Gas content and gas concentration in the southwestern Ordos Basin.

$CH_4$, δD-$CH_4$, $\delta^{13}$C-$CO_2$, CDMI, and $R_{o,max}$ are used to comprehensively evaluate the genetic type of gas and improve the accuracy of identification (Fu et al., 2019; Zhang et al., 2019b).

### 3.3.1 Source of methane in CBM

The $\delta^{13}$C-$CH_4$ value and the $C_1/(C_2H_4 + C_3H_6)$ ratios of the gas samples (Table 2) in the study area were plotted using the Whiticar (1999) chart to investigate the genetic type of $CH_4$ (Fig. 7). The $CH_4$ component in CBM from Binchang mining area are all biogenic genetic types, and the $CH_4$ samples form Huangling and Jiaoxun mining areas are biogenic gas and mixed genetic gas. The genetic type of $CH_4$ in the Yonglong mining area is mainly biogenic gas, but one data point belongs to thermogenic gas. The genesis types of $CH_4$ in the Longdong mining area are all thermally generated gas. On the whole, the $\delta^{13}$C-$CH_4$ value increases from the edge to the interior of the basin. The shallow CBM in the southern edge of the basin is mainly biogenic gas, and some mining areas contain a small amount of mixed genetic gas, while the deep CBM in the Longdong mining area in the north is all thermogenic gas.

Biogenic gas includes two genetic mechanisms: $CO_2$ reduction and methyl fermentation (Whiticar, 1999), and the corresponding $\delta^{13}$C-$CH_4$ interval values are approximately −55 ‰ to −110 ‰ and −40 ‰ to −70 ‰, respectively (Rice, 1993). Moreover, the δD-$CH_4$ value ( −250‰ to −400‰) of methyl fermentation is lower than the δD-$CH_4$ value ( −150‰ to −250‰) of $CO_2$ reduction (Fu et al., 2019). Hence, the values of $\delta^{13}$C-$CH_4$ and δD-$CH_4$ are important indicators to identify the genetic type of $CH_4$. In Fig. 8, the origin of biogenic methane in the study area is generated by the $CO_2$ reduction path, consistent with the major low-rank CBM basins (Bowen, San Juan, and Surat basins) in the world (Li et al., 2015; Fu et al., 2019).

In the geological history, CBM will not only escape but also be oxidized and degraded by bacteria. Although the carbon isotope fractionation caused by the bacteria oxidative degradation of $CH_4$ is smaller than that caused by the formation of SBG. This variation may still affect the identification of the formation mechanism of CBM on the $\delta^{13}$C-$CH_4$ versus δD-$CH_4$ curves (Whiticar, 1999; Ju et al., 2014). Thus, the plot of $\delta^{13}$C-$CH_4$ versus $\delta^{13}$C-$CO_2$ was used to further study the biogenic gas generation pathway. Figure 9 shows that all samples from the Binchang mining area are in the $CO_2$ reduction zone; the Jiaoxun and Yonglong mining areas are in the methyl fermentation zone; the Huangling mining area contains two types. This judgment result is consistent with the $\delta^{13}$C-$CH_4$ versus δD-$CH_4$ plate (Fig. 8). The biogenic gas in the Binchang mining area is formed by $CO_2$ reduction,

**Table 2** Stable isotopic values of CBM samples in the southwestern Ordos Basin

| Mining area | Well | *H*/m | $R_o$/% | Hydrocarbon index | Isotope values/‰ | | | CDMI/% | Source |
|---|---|---|---|---|---|---|---|---|---|
| | | | | $C_1/(C_2+C_3)$ | $\delta^{13}C$ ($CO_2$) | $\delta^{13}C_1$ (PDB) | δD (SMOW) | | |
| Yonglong | GJH-01 | 553 | 0.51 | 265 | −23.2 | −56.5 | −205.8 | 0.13 | This work |
| | QJP-01 | 624 | 0.51 | 10000 | −18.8 | — | — | — | |
| | YZG2-1 | 664 | 0.58–0.63 | 1361 | — | −55.1 | −236.3 | 0.03 | |
| | YZG2 | 672 | | 562.25 | −34.0 | −48.0 | −238.3 | 0.07 | |
| | YZG3 | 690 | | 3457 | −14.7 | — | — | 0.01 | |
| Binchang | DFS01 | 507 | 0.60–0.65 | n | n | −72.2 | −235 | n | Jin and Zhang (2014) |
| | DFS02 | 511 | | n | n | −72.7 | −236 | n | |
| | DFS03 | 570 | | n | n | −71.9 | −235 | n | |
| | DFS04 | 579 | | n | n | −80.0 | −235 | n | |
| | DC01 | 513 | 0.60–0.65 | 7468 | −23.1 | −80.7 | −242.6 | 0.02 | This work |
| | DM-68 | 498 | | 7856 | −5.0 | −70.1 | −244.1 | 0.01 | |
| | DM-143 | 485 | | 7816 | −13.4 | −75.5 | −246.0 | 0.01 | |
| | DM-68 | 498 | 0.60–0.65 | 7788 | −13.2 | −68.9 | −239.9 | 0.83 | Bao et al. (2020) |
| | DM-69 | 490 | | 7788 | −20.3 | −82.3 | −241.4 | 0.99 | |
| | DM-05 | 504 | | 7788 | −14.8 | −76.5 | −240.7 | 1.65 | |
| | DM-148 | 592 | | 7788 | −32.9 | −86.5 | −243.7 | 1.87 | |
| | DM-133 | 566 | | 7788 | −36.6 | −87.2 | −245.5 | 2.67 | |
| | DM-128 | 582 | | 7788 | −22.7 | −83.7 | −242.3 | 2.33 | |
| | DM-09 | 584 | | 10000 | — | −73.7 | −236.6 | 0.31 | |
| | DM-131 | 583 | | 7734 | — | −77.6 | −243.5 | 0.40 | |
| | DM-45 | 584 | | 7033 | — | −76.1 | −243.1 | 0.62 | |
| | XZ01 | 400–470 | 0.60–0.63 | n | n | −80.6 | n | n | Zhang et al. (2020) |
| | XZ02 | | | n | n | −70.1 | n | n | |
| | XZ03 | | | n | n | −69.1 | n | n | |
| | XZ04 | | | n | n | −73.1 | n | n | |
| | XZ05 | | | n | n | −75.3 | n | n | |
| | XZ06 | | | n | n | −69.6 | n | n | |
| | XZ07 | | | n | n | −71.1 | n | n | |
| | XZ08 | | | n | n | −73.1 | n | n | |
| Jiaoxun | JP01 | 507 | 0.56 | 9000 | n | −57.6 | −250.0 | n | Jin and Zhang (2014) |
| | JP02 | 543 | 0.60 | 183 | n | −56.9 | −250.0 | n | |
| | CJG-01 | 518 | 0.55 | 52 | −20.40 | −55.4 | −218.9 | 0.04 | This work |
| Huangling | HL01 | 855 | 0.89 | 96 | n | −54.5 | −250.0 | n | Jin and Zhang (2014) |
| | HL02 | 350 | 0.78 | 10000 | n | −68.8 | −244.0 | n | |
| | HL03 | 451 | 0.79 | 99 | n | −59.9 | −248.0 | n | |
| | HL04 | 350 | 0.78 | 10000 | n | −69.0 | −251.0 | n | |
| | HL05 | 350 | 0.78 | 10000 | n | −68.9 | −250.0 | n | |
| | HL-Z | 450–550 | 0.78 | n | −26.91 – −11.50 | −70.3 – −56.2 | −268.0 – −223.9 | n | Zhao et al. (2018) |
| | HL2-1 | 500 | 0.75 | 491 | — | −55.2 | −206.9 | 0.01 | This work |
| Longdong | QY01 | 1068 | 0.79 | 22 | n | −46.5 | −243.0 | 0.10 | Jin and Zhang (2014) |
| | QY02 | 1110 | 0.79 | 15 | n | −47.9 | −264.0 | | |
| | QY03 | 1140 | 0.79 | 21 | n | −48.5 | −263.0 | | |
| | QY04 | 1136 | 0.79 | 82 | n | −33.1 | −268.0 | | |
| | HN-T | ＞1000 | 0.79 | n | n | −32.5 – −49.0 | n | 0.10 | Tian et al. (2015) |

Note: "n" = no data; "—"= not detected; CDMI = $[CO_2/(CO_2 + CH_4)] \times 100\%$.

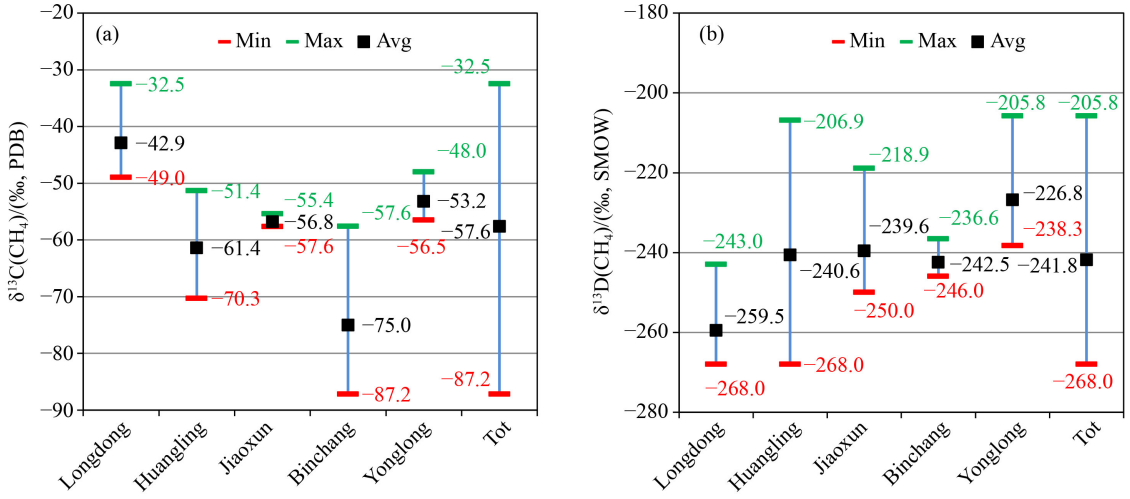


**Fig. 4** Statistical charts of stable isotopic values of CBM samples in the southwestern Ordos Basin.

**Table 3** Hydrochemical characteristics of coalbed water in the southwestern Ordos Basin

| Mining area | Well | Ion content/(mg·L$^{-1}$) | | | | | | | | TDS/ (mg·L$^{-1}$) | PH | Water types | Permeability/ (mD) |
|---|---|---|---|---|---|---|---|---|---|---|---|---|---|
| | | $Ca^{2+}$ | $Mg^{2+}$ | $Na^{+}$ | $K^{+}$ | $HCO_3^{-}$ | $SO_4^{2-}$ | $Cl^{-}$ | $CO_3^{2-}$ | | | | |
| Yong long | k4-4 | 26.05 | 18.91 | 474.76 | | 230.26 | 690.45 | 190.00 | 0 | 1631.00 | 8.00 | Na–$SO_4$ | 0.01–0.66 |
| | k3-9 | 17.60 | 11.67 | 400.14 | | 197.86 | 83.97 | 515.46 | 0 | 1232.10 | 8.40 | Na–Cl | 0.16 |
| | Z9-5 | 36.33 | 17.53 | 190.00 | | 306.37 | 303.35 | 25.00 | 0 | 879.98 | 8.20 | Na–$SO_4$ | |
| | Z10-4 | 43.85 | 18.00 | 143.82 | | 282.40 | 223.50 | 21.17 | 0 | 734.49 | 8.15 | Na–$SO_4$ | |
| Bin chang | C01-1 | 65.80 | 46.80 | 4659.00 | 0 | 1683.00 | 31.00 | 6539.00 | 0 | 13020.00 | 7.9 | Na–Cl | 0.09–5.73 |
| | C01-2 | 58.72 | 37.05 | 4580.00 | 111.00 | 1492.00 | 5.24 | 6291.00 | 13 | 12588.50 | 7.86 | Na–Cl | 2.07 |
| | M68 | 75.39 | 31.76 | 2940.00 | 26.00 | 975.60 | 20.90 | 4072.00 | 0 | 8142.00 | 7.77 | Na–Cl | |
| | M143 | 331.70 | 130.4 | 3800.00 | 40.80 | 1019.00 | 17.42 | 5946.00 | 0 | 11285.00 | 7.26 | Na–Cl | |
| | B1 | 361.10 | 89.68 | 3820.00 | 21.50 | 383.80 | 6969.00 | 1527.00 | 0 | 13179.90 | 7.72 | Na–$SO_4$ | |
| | B2 | 369.10 | 90.41 | 4280.00 | 20.89 | 390.90 | 7504.00 | 1598.00 | 0 | 14278.90 | 7.76 | Na–$SO_4$ | |
| | XZ1 | 101.48 | 21.20 | 3840.72 | 18.25 | 692.52 | 5163.58 | 2293.43 | 13.34 | 12144.86 | n | Na–$SO_4$ | |
| | GJB-1 | 447.38 | 124.50 | 4233.67 | 26.30 | 310.53 | 8155.33 | 1539.15 | 1.13 | 14850.67 | n | Na–$SO_4$ | |
| Jiao xun | JP1 | 21.24 | 18.93 | 1728.91 | 173.94 | 1936.43 | 46.13 | 1630.13 | 0 | 5560.86 | 7.90 | Na–Cl | 0.01–3.00 |
| | JP2 | 19.50 | 16.32 | 1533.00 | 3.06 | 1631.27 | 33.75 | 1479.12 | 0 | 4769.00 | 8.46 | Na–Cl | 1.21 |
| | JP3 | 28.82 | 16.17 | 1508.00 | 3.83 | 1727.63 | 23.46 | 1424.52 | 0 | 4734.00 | 8.41 | Na–Cl | |
| | JP4 | 25.74 | 15.19 | 1620.00 | 4.51 | 1466.08 | 31.69 | 1687.59 | 0 | 4890.00 | 8.41 | Na–Cl | |
| Huang ling | HK1 | 258.61 | 71.54 | 2921.63 | | 266.82 | 6329.38 | 349.54 | 0 | 10199.98 | n | Na–$SO_4$ | 1.03–3.65 |
| | HK2 | 132.48 | 51.60 | 825.07 | | 602.04 | 1647.63 | 89.12 | 0 | 3351.98 | n | Na–$SO_4$ | 2.43 |
| Long dong | N2 | 557.00 | 451.00 | 17554.00 | 0 | 1967.00 | 1336.00 | 26579.00 | 0 | 48440.00 | 6.00 | Na–Cl | 0.04–1.19 |
| | N28 | 805.00 | 451.00 | 13299.00 | 0 | 1117.00 | 594.00 | 22149.00 | 0 | 38420.00 | 6.00 | Na–Cl | 0.32 |
| | XS1 | 495.00 | 376.00 | 16973.00 | 0 | 1339.00 | 1187.00 | 26478.00 | 0 | 46850.00 | 6.00 | Na–Cl | |
| | XF1 | 403.5 | 231.50 | 75000.00 | 137.21 | 350.50 | 251.00 | 271.10 | 0 | 76646.00 | 6.35 | Na–Cl | |
| | XF 2 | 337.58 | 203.32 | 58300.00 | 195.82 | 627.40 | 150.60 | 260.30 | 0 | 60077.00 | 6.57 | Na–$HCO_3$ | |
| | XF 4 | 574.32 | 235.23 | 49700.00 | 227.85 | 761.40 | 116.00 | 293.70 | 0 | 51910.00 | 6.96 | Na–$HCO_3$ | |
| | XF 5 | 405.20 | 233.21 | 56300.00 | 144.60 | 405.20 | 243.50 | 104.00 | 0 | 57836.00 | 6.51 | Na–$HCO_3$ | |
| | XF 6 | 371.58 | 196.37 | 92300.00 | 183.67 | 258.96 | 294.20 | 291.80 | 0 | 93898.00 | 6.31 | Na–Cl | |

Notes: TDS = total dissolved solid; “n” = no data.

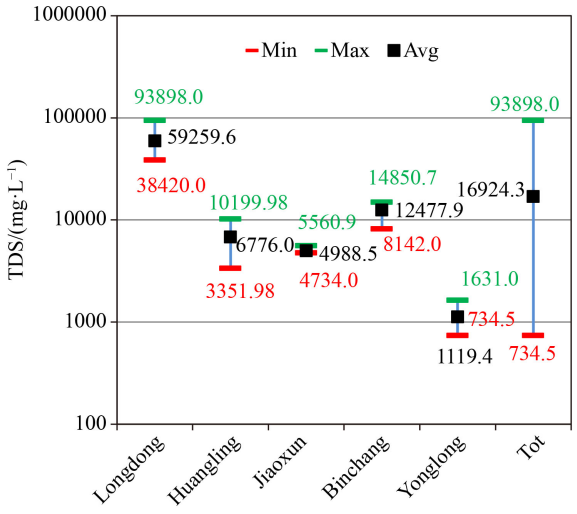


**Fig. 5** TDS statistical chart of hydrochemical characteristics in the southwestern Ordos Basin.

while the other mining areas are formed by methyl fermentation. $CO_2$ reduction mainly happens in saltwater environments, whereas methyl fermentation occurs in a freshwater environment (Vinson et al., 2017). The methanogenesis mechanism is affected by two factors. On the one hand, hydrotrophic methanogenesis is more salt-tolerant than acetoclastic methanogenesis, and on the other hand, sulfate in salt water can completely inhibit the competitive substrates used by methanogens. After sulfate reducing agents run out of available acetate, hydrotrophic methanogenesis takes a leading position (Whiticar et al., 1986;Vinson et al., 2017; Fu et al., 2022). The TDS of coalbed water in the Binchang mining area is generally greater than 10000 mg/L (Table 3), which has the conditions to generate biogenic gas by $CO_2$ reduction.

### 3.3.2 Source of carbon dioxide in CBM

$CO_2$ can be classified as organic genetic and inorganic genetic, where organic genetic originates from two mechanisms: $CO_2$ associated with hydrogen oxidation and thermal $CO_2$ generated (Kotarba and Rice, 2001). In the study area, the $\delta^{13}C$-$CO_2$ value is distributed from −36.6 ‰ to −5.0 ‰, with a large variation range. According to the plot of the $(CO_2/[CO_2 + CH_4]) \times 100\%$ (CDMI) value versus $\delta^{13}C$-$CO_2$ value, the genetic of $CO_2$ in CBM can be judged (Kotarba and Rice, 2001). In Fig. 10, the $CO_2$ in CBM is organic gas and mainly thermogenic $CO_2$ in the study area. Individual gas samples in the Binchang and Yonglong mining areas contain $CO_2$ related to hydrocarbon oxidation. The differential genetic of $CO_2$ in the study area are mainly controlled by the differences of coal metamorphism, coal reservoir permeability and tectonic evolution.

## 4 Discussion

### 4.1 Influence of tectonic evolution on the generation of CBM

The generation mechanism of CBM is very complicated (Tao et al., 2021; Wang et al., 2022). The formation and evolution of the CBM are affected by the composition characteristics of source rock, depositional environments, burial conditions, tectonic-thermal evolution process,

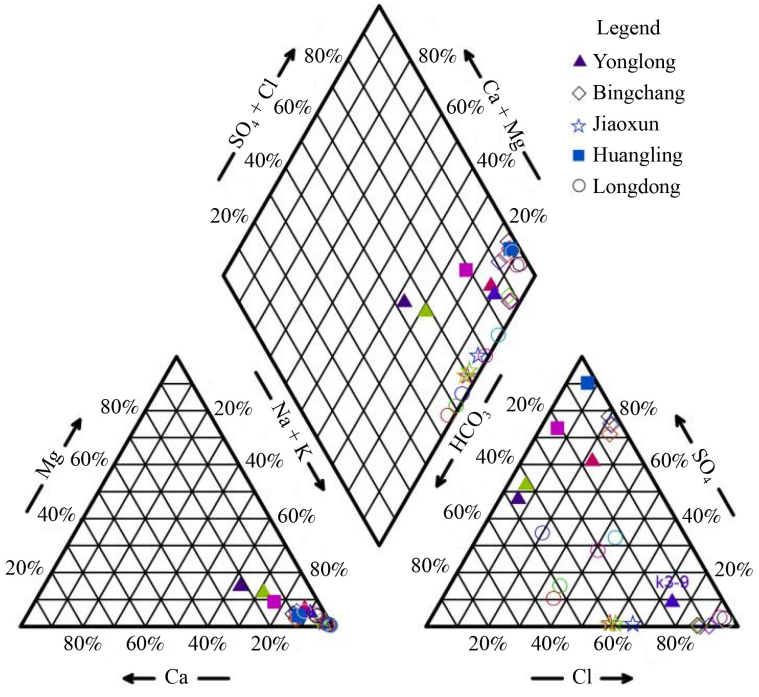


**Fig. 6** Piper diagram of the major ions of coalbed water in the southwestern Ordos Basin.

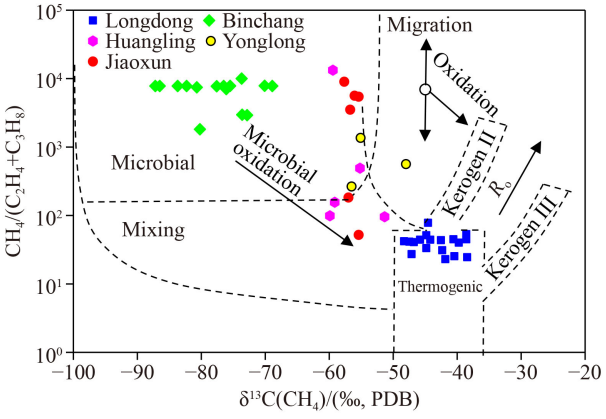


**Fig. 7** Diagram showing the combined methane $\delta^{13}C\text{-}CH_4$ and $CH_4/(C_2H_4 + C_3H_6)$. Modified from Whiticar (1999).

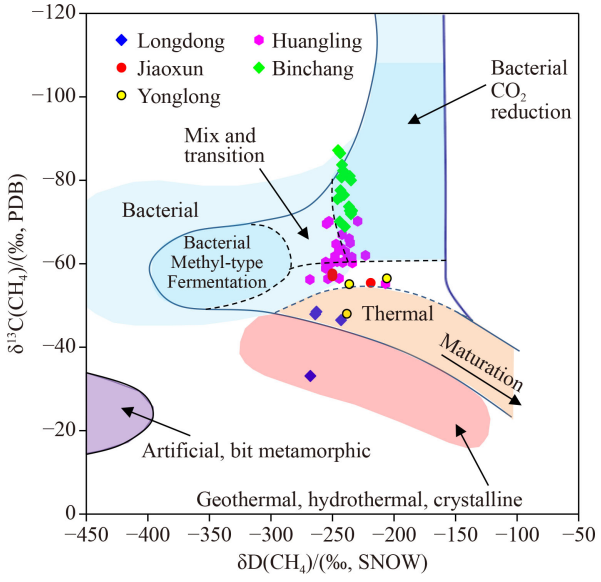


**Fig. 8** Genetic judgment of $CH_4$ by $\delta D\text{-}CH_4$ and $\delta^{13}C\text{-}CH_4$. Modified from Whiticar (1999).

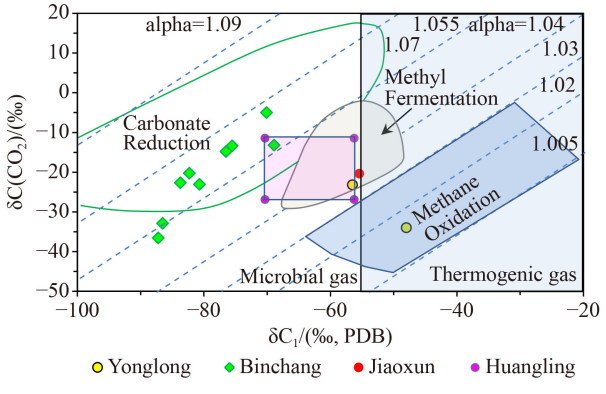


**Fig. 9** Diagram showing combined methane $\delta^{13}C\text{-}CH_4$ and $\delta^{13}C\text{-}CO_2$ to identify the origin of gas. Modified from Whiticar (1999).

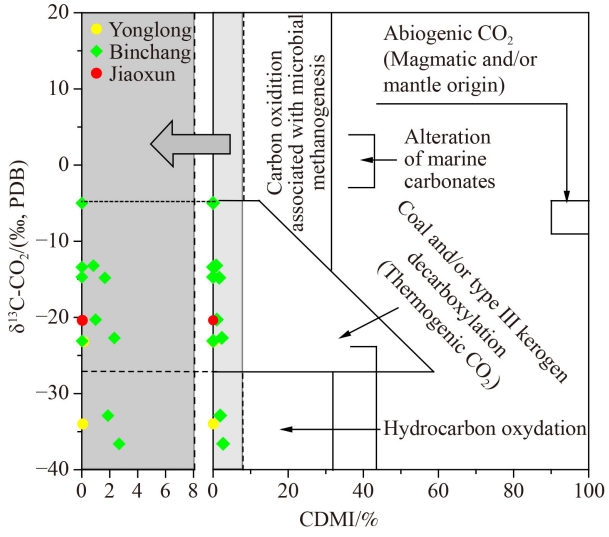


**Fig. 10** Diagram showing combined $\delta^{13}C\text{-}CO_2$ and $[CO_2/(CH_4 + CO_2)] \times 100\%$ (CDMI). Modified from Kotarba and Rice (2001).

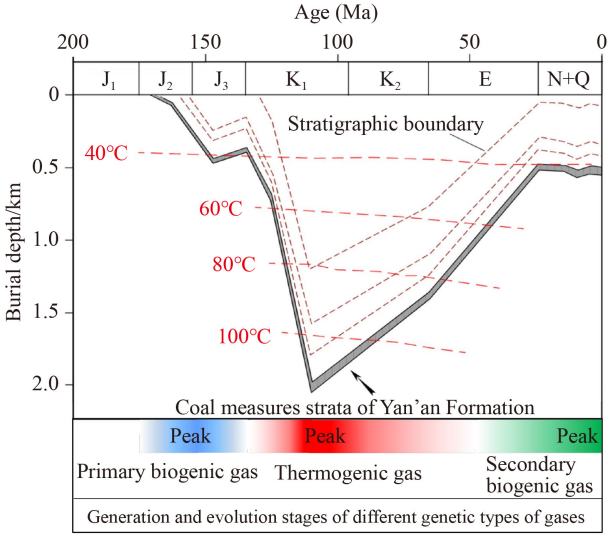


**Fig. 11** Hydrocarbon generation and evolution history of coal measure strata of Yan'an formation in the southwestern Ordos Basin (Modified from Lin, 2021a).

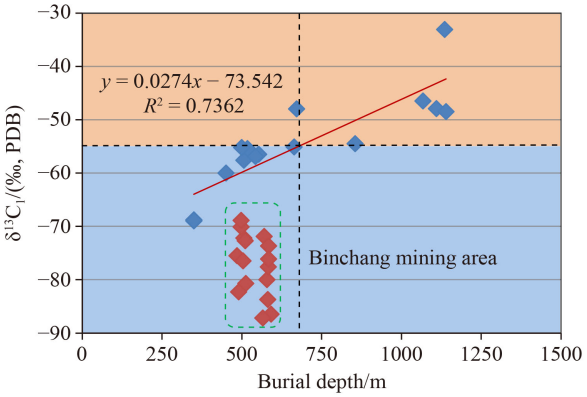


**Fig. 12** Diagram showing combined $\delta^{13}C\text{-}CH_4$ versus burial depth.

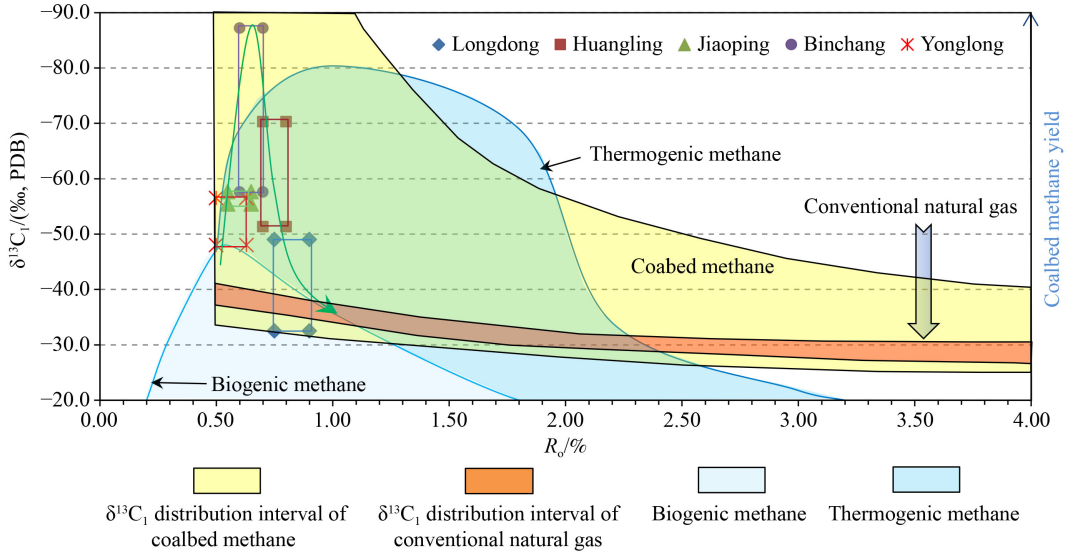


**Fig. 13** Different distributions of $\delta^{13}C$-$CH_4$ value of conventional natural gas and CBM. Modified from Dai (1986) and Moore (2012).

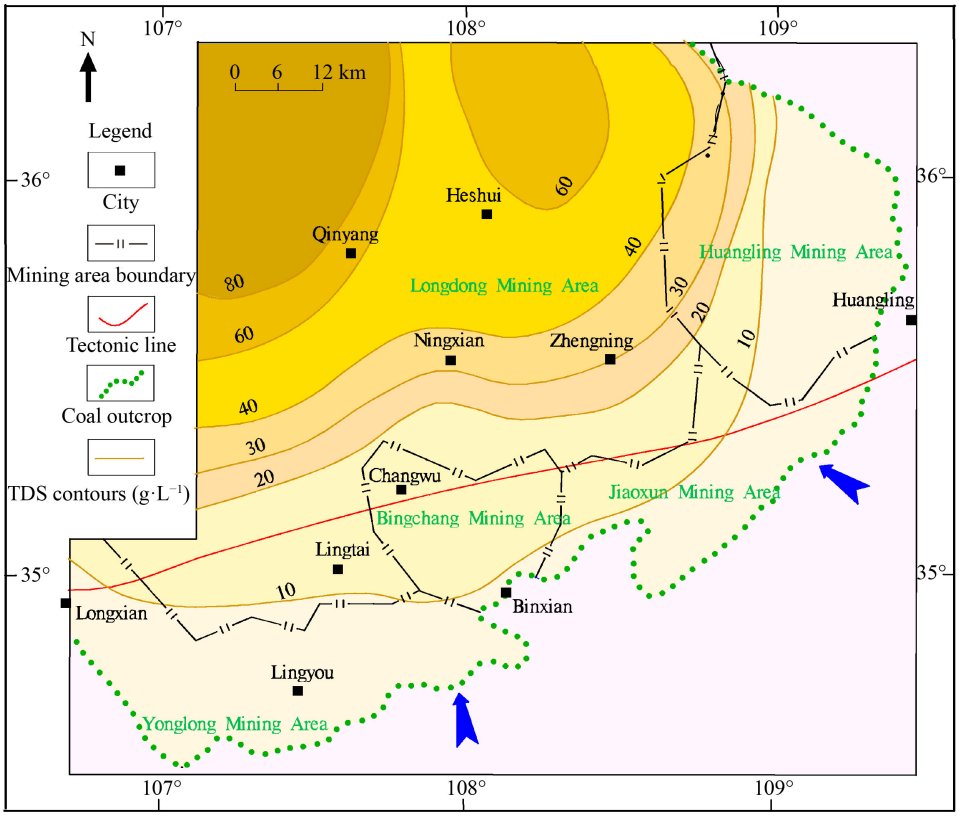


**Fig. 14** The contour map of the TDS values of the Yan'an Formation groundwater in the southwestern Ordos Basin.

microorganisms, and hydrodynamic force (Zhang et al., 2019b; Lan et al., 2020). The geological period of the highest peak of coal seam thermal evolution often determines the geochemical characteristics of CBM (Wang et al., 2022). The simulation results of the burial and thermal history of coal-bearing strata of Yan'an Formation show that the coal-bearing strata experienced two periods of uplift and subsidence, which had an important impact on the hydrocarbon generation history of the coal (Fig. 11). During the first phase of the Yanshanian orogeny, the 4th and 5th members at the top of the Yan'an formation suffered denudation. Since then, the study area was uplifted again in the Phase II of Yanshanian orogeny (Late Jurassic), resulting in loss of deposits of most of the upper Jurassic stratigraphy and escape of most of the primary biogenic gas. In the Phase

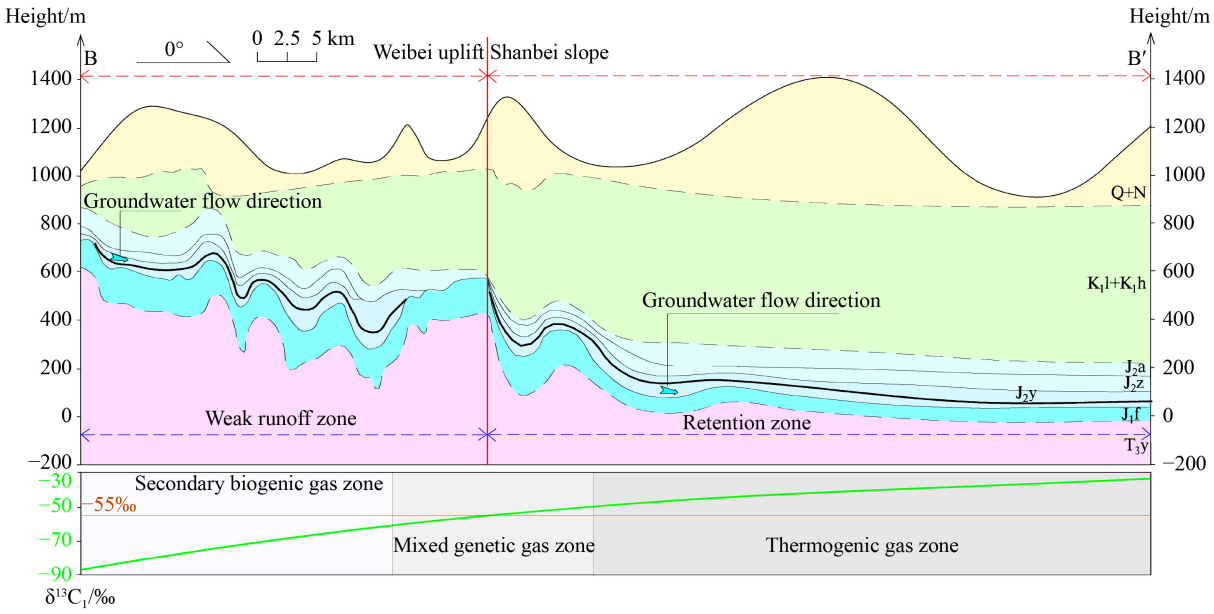


**Fig. 15** Cross section (BB′) of the CBM genetic type under hydrodynamic and tectonic conditions (the section line can be found in Fig. 1).

III of Yanshanian orogeny (Early Cretaceous), the south-western Ordos Basin subsided rapidly. At this time, the burial depth of Yan'an formation reached the maximum (about 2000 m), and the burial depth of the Huangling mining area was the largest. Simultaneously, the temperature of the coal reservoir had reached the maximum (the max temperature reached 105°C), and the max temperature of the coal reservoir on the plane had the characteristics of high in the south and low in the north. At this time, the peak of thermogenic gas generation was formed. In the Phase IV of Yanshanian orogeny, the Ordos Basin was fully uplifted, ending the deposition of the large depression basin. During this process, the overlying strata of the coal reservoir were eroded, and the pressure of the reservoir decreased, resulting in the escape of a large amount of thermogenic gas. This indicates that the uplift of Yan'an Formation strata between the Late Cretaceous and Paleogene caused the escape of early thermal gas. As a result, the proportion of thermogenic gas in the basin edge of the study area is low, and this has an important impact on the geochemical characteristics of CBM in the south-western Ordos Basin. Since the Paleogene Period, the southern margin of the Ordos Basin has received recharge from atmospheric precipitation, and the SBG has begun to generate.

### 4.2 Influence of burial depth and thermal evolution on the generation of CBM

The origin of CBM in the south-western Ordos Basin are diverse, which mainly originates from the differences in tectonic location, coalification degree, and groundwater activity in different mining areas. Although the tectonic is generally simple in the study area, the difference in coal seam burial depth caused by the tectonic has an obvious impact on the geochemical characteristics of CBM (Figs. 3 and 5). In Fig. 12, $\delta^{13}$C-$CH_4$ increases linearly with increasing burial depth, except the Binchang mining area. Zhang et al. (2019a) also found a similar phenomenon in the eastern Ordos Basin. This is due to different fractionation phenomena in the CBM escape process (Qin et al., 2000). When the basin uplifted, the coal reservoir pressure decreased, and the carbon isotope of $CH_4$ with different neutron numbers desorbed, diffused, and migrated, resulting in isotopic fractionation. However, the correlation between $\delta^{13}$C-$CH_4$ and burial depth in the Binchang mining area is poor, indicating that the vertical fractionation of CBM is weak. This is due to the high salinity of coalbed water and weak hydrodynamic conditions in the Binchang mining area. CBM is not easy to dissolve in high salinity water, and the generated biogenic gas is strongly lateral sealed by coalbed water. Previous studies have shown that biogenic gas generally occurs in coal seams with a burial depth of less than 800 m, but there are differences in different regions (Whiticar, 1999). In Fig. 12, the conversion depth of biogenic gas versus thermogenic gas in the south-western Ordos Basin is about 660 m, indicating that the favorable occurrence depth of biogenic gas is less than 660 m. When the burial depth is greater than 1000 m, the gas types are all thermogenic gas.

Burial depth is only a spatial concept. The temperature and pressure related to the burial depth affect the degree of coal metamorphism and hydrogeological conditions (including water quality characteristics and coal reservoir permeability), which in turn become the key factors affecting the geochemical characteristics of CBM (Li

et al., 2019). The study area is plutonic metamorphic coal. Except for the eastern Huangling mining area, the degree of coal metamorphism gradually increases with increasing burial depth (Fig. 1). Generally, with increasing degree of coalification, $\delta^{13}C\text{-}CH_4$ increases (Dai et al., 1986; Zhang et al., 2019b). However, the $\delta^{13}C\text{-}CH_4$ value first decreased and then increased with the increased $R_o$ (Fig. 13), which is obviously different from the previous understanding. This is because the gas of the Binchang mining area is a pure biogenic gas, which causes the $\delta^{13}C\text{-}CH_4$ value to be lower in the stage of 0.60%–0.70% ($R_o$). The vitrinite reflectance in the study area is 0.50%–0.93%, which is in the middle and late stages of SBG and the early and middle stages of thermogenic gas (Fig. 13). With increasing $R_o$, the contribution of biogenic gas gradually decreases, while the thermogenic gas gradually increases. However, if the thermal evolution of coal stops, the basin margin has favorable geological conditions for the formation of biogenic gas, and the large replenishment of SBG will change the positive correlation between the $\delta^{13}C\text{-}CH_4$ value and $R_o$.

### 4.3 Influence of hydrogeological conditions on the generation of CBM

Hydrogeological conditions have an important impact on the generation and enrichment of CBM (Rice and Claypool, 1981; Scott et al., 1994; Kotarba and Rice, 2001; Fu et al., 2021). The physicochemical and microbial activities of groundwater have an important impact on the formation and migration of CBM (Zhou et al., 2020). In the horizontal and vertical sections, the areas with strong hydrodynamic conditions not only have relatively low CBM content but also have lighter $\delta^{13}C\text{-}CH_4$ values (Qin et al., 2006). The borehole pumping test shows that the water of Yan'an formation in the south-western Ordos Basin is mainly supplied by surface water from the outcrop along the stratum, and the vertical supply is weak (Lin et al., 2021a). The groundwater salinity increases gradually with the increased stratum burial depth (Fig. 14). The lateral recharge of water in the Yan'an formation is mainly comes from the outcrop areas in the east and south. Surface fresh water enters the basin along the NW direction. The ground hydrodynamic conditions gradually weakened with increasing burial depth, and the TDS of formation water increased. The type of water quality transitioned from $Na_2SO_4$ type to $NaHCO_3$ type water, up to $CaCl_2$ type water (Dong, 2010). Because Longdong mining area is located in the retention area of deep hydrodynamic field of the basin, the TDS in this area is obviously higher than that of other mining areas at the edge of the basin. In each mining area, the difference of geological conditions of coal seam outcrop leads to the difference of surface water recharge intensity. Therefore, the TDS and water quality types of each mining area at the edge of the basin are different.

The formation conditions of SBG are strict (Rice and Claypool, 1981). Biogenic gas generally requires a suitable type of gas-producing parent material ($R_o$ at 0.3%–1.5%), lower temperature (< 50°C), strong reducing environment, low salinity water (the $SO_4^{2-}$ concentration is < 960 mL/g, and TDS is < 10000 mg/L), and neutral pH (Rice and Claypool, 1981; Whiticar et al., 1986; Green et al., 2008; Fu et al., 2019).

Compared with the above conditions, the Yonglong, Binchang, Jiaoxun, and Huangling mining areas are located at the edge of the basin, and there are conditions for the formation of biogenic gas in structure and depth. However, SBG is only formed on a large scale in the Binchang mining area, while it is formed on a small scale in the Yonglong, Jiaoxun, and Huangling mining areas. The difference of kerogen types in Yan'an formation is small, and the hydrogeological conditions are the key controlling factor affecting the formation of biogenic $CH_4$ differences. The Longdong mining area is located in the coalbed water retention zone in the deep part of the basin. The extremely high TDS water is conducive to the propagation and growth of sulfate-reducing bacteria, resulting in acidic coal seam water. Therefore, it does not have the generation conditions for biomethane. In the Yonglong mining areas, the chemistry type of coalbed water is Na-$SO_4$ type and the permeability of coal reservoir is low, which is not conducive to the formation of biomethane. The water chemistry type in the Jiaoxun and Binchang mining areas is Na–Cl, but the pH of the water in the Jiaoxun mining area is weakly alkaline. TDS is generally greater than 10000 mg/L in the Binchang mining area, but the pH value of water is neutral. Meanwhile, the permeability of the coal reservoir is high (Lin, 2021), which has favorable conditions for the formation of biomethane. Although the coal reservoir permeability in Huangling mining area is also high (Table 3), the water quality type is Na–$SO_4$ and the thickness of coal seam is small. Hence it does not have the best conditions for the formation of biomethane. The type of water quality of the Yan'an formation in the Binchang and Jiaoxun mining areas in the study area is similar to those of the Walloo coal measures in the Surat Basin, Australia, the genetic types of which are also biogenic gas (Tang et al., 2018). It indicates that the water quality type of Na–Cl is favorable for the formation and enrichment of biogenic gas.

### 4.4 Generation geological model of CBM and its significance to CBM development

In the south-western Ordos Basin, the burial depth gradually increases from south-east to north-west, as well as the degree of coal metamorphism and hydrodynamic condition variation (Fig. 1), leading to differences in the generation and evolution environment of CBM. Since the

late Paleogene Period, the basin margin has been recharged by atmospheric precipitation, which is conducive to the formation of biogas. A generation geological model of CBM was established by taking the central area of the study area as an example (Fig. 15) which is bounded by the Shanbei slop and the Weibei uplift tectonic line. The hydrodynamic field can be divided into the southern weak runoff zone and the northern stagnation zone (Fig. 15). The Binchang mining area is located in the southern weak runoff zone of groundwater, and the SBG is formed by $CO_2$ reduction. For the northern Longdong mining area, the burial depth of coal reservoir is large, and it is located in the retention zone of groundwater, thus, it does not have the geological conditions for the generation of SBG. Therefore, the CBM source in deep areas is mainly the residual gas of early thermal origin, and the intermediate transition zone is the mixed gas. The CBM of the Huangling, Jiaoxun, and Yonglong mining areas comes from the early thermogenic gas and later superimposed SBG, which is affected by the comprehensive effects of coal metamorphism, geological structure, and hydrology. Due to the thermal gas escaping from the deep basin in the late Mesozoic and the lack of favorable conditions for the formation of biogenic gas since the Cenozoic, the gas content in the study area gradually decreases with the burial depth after exceeding the optimal generation depth of biogenic gas (Fig. 3(a)). Based on the current CBM development results, the development of biogenic gas in the Binchang mining area has been successful. Accordingly it can be concluded that looking for coal reservoirs with similar conditions for the formation of biogenic gas at the edge of the basin is key to the successful development of CBM in the south-western Ordos Basin.

## 5 Conclusions

1) The gas content in the south-western Ordos Basin is distributed in the range of 0.01–6.31 $m^3/t$ (av. 2.08 $m^3/t$), with the component content of $CH_4$ in the range of 42.01%–94.72%. The concentration of heavy hydrocarbon gas is 0%–6.74%, which is extremely low in the Binchang and Jiaoxun mining area. The $\delta^{13}C\text{-}CH_4$ value in the whole south-western Ordos Basin is distributed from −87.2 ‰ to −32.5 ‰ (av. −57.6 ‰). The $\delta D\text{-}CH_4$ value is distributed from −268.0 ‰ and −205.8 ‰ (av. −214.8 ‰). The $\delta^{13}C\text{-}CO_2$ value is distributed from −36.6‰ to −5.0‰ (av. −20.9‰).

2) The $CH_4$ in the Binchang mining area is biogenic gas, while that in the Yonglong, Jiaoxun, and Huangling mining areas are mixed genetic gas, and that in the Longdong mining area is thermogenic gas. The microbial methane in the study area are mainly from the microbial $CO_2$ reduction path. The $CO_2$ concentration in the study area is 0.32%–14.44%, which is mainly thermogenic gas, and $CO_2$ associated with microbial methanogenesis is found in individual points in the Binchang and Yonglong mining areas.

3) The Yanshanian orogeny in the Late Cretaceous caused an overall uplift of the Ordos Basin, resulting in the escape of early thermogenic gas at the south-western basin. Except for the Binchang mining area, the $\delta^{13}C\text{-}CH_4$ value has a positive linear correlation with burial depth in the whole south-western Ordos Basin. The CBM in the Binchang mining area is laterally sealed by coalbed water, and the vertical fractionation of CBM is weak. Moreover, the favorable burial depth for the formation of biogenic gas in the study area is within 660 m.

4) Affected by the SBG, the $\delta^{13}C\text{-}CH_4$ value of CBM first decreases and then increases with increasing $R_o$, which is obviously different from the past monotonic increasing function. The genetic types of gas in the different mining areas are affected by tectonic setting, burial depth, coal rank, and hydrogeology. A generation geological model of CBM was established, and it indicates that coal reservoirs with similar conditions for the formation of biogenic gas is key to the successful development of CBM in the south-western Ordos Basin.

**Acknowledgment** This work was financially supported by the National Natural Science Foundation of China (Grant Nos. 42130802 and 42372200), China Postdoctoral Science Foundation (No. 2022M713792), Key Science and Technology Program of Shaanxi Province (No. 2023YBGY-083), and Open Fund of Key Laboratory of Coalbed Methane Resources and Reservoir Formation Process of the Ministry of Education (China University of Mining and Technology) (No. 2022-007).

**Competing interests** The authors declare that they have no competing interests.

## References

Bao Y, Wang W, Ma D, Shi Q, Ali A, Lv D, Zhang C (2020). Gas origin and constraint of $\delta^{13}C(CH_4)$ distribution in the Dafosi mine field in the southern margin of the Ordos Basin, China. Energy Fuels, 34(11): 14065–14073

Chen Y, Qin Y, Ji M, Duan H, Wu C, Shi Q, Zhang X, Wang Z (2020). Influence of lamprophyre sills on coal metamorphism, coalbed gas composition and coalbed gas occurrence in the Tongxin Minefield, Datong Coalfield, China. Int J Coal Geol, 217: 103286

Conrad R (2005). Quantification of methanogenic pathways using stable carbon isotopic signatures: a review and a proposal. Organic Geochem, 36(5): 739–752

Dai J, Qi H, Song Y, Guan D (1986). The components and carbon isotopes of coal bed gases in China and origin. Sci China Series B-Chem, Bio, Agri, Med Earth Sci, 16(12): 1317–1326 (in Chinese)

Dong J (2010). The rule of the coal accumulation and coal-bed methane accumulation in Jurassic Yan'an Formation of Ordos Basin. Dissertation for Master's Degree. Qingdao: China University of Petroleum

Fu H, Tang D, Pan Z, Yan D, Yang S, Zhuang X, Li G, Chen X, Wang G (2019). A study of hydrogeology and its effect on coalbed methane enrichment in the southern Junggar Basin, China. AAPG Bull, 103(1): 189–213

Fu H, Yan D, Su X, Wang J, Li Q, Li X, Zhao W, Zhang L, Wang X, Li Y (2022). Biodegradation of early thermogenic gas and generation of secondary microbial gas in the Tieliekedong region of the northern Tarim Basin, NW China. Int J Coal Geol, 261: 104075

Fu H, Yan D, Yang S, Wang X, Wang G, Zhuang X, Zhang L, Li G, Chen X, Pan Z (2021). A study of the gas-water characteristics and their implications for the coalbed methane accumulation modes in the southern Junggar Basin, China. AAPG Bull, 105(1): 189–221

Green M S, Flanegan K C, Gilcrease P C (2008). Characterisation of a methanogenic consortium enriched from a coalbed methane well in the Powder River Basin, USA. Int J Coal Geol, 76(1–2): 34–45

Gutsalo L K (2008). Isotope fractionation in the systems $CH_4$–$H_2O$ and $CH_4$–$CO_2$ during microbial methane genesis in the Earth's crust. Russ Geol Geophys, 49(6): 397–407

Jin X, Zhang H (2014). Evolution of Jurassic low rank coal CBM system in Ordos basin. Coal Geol Explor, 42: 17–24

Ju W, Yang Z, Shen Y, Yang H, Wang G, Zhang X, Wang S (2021). Mechanism of pore pressure variation in multiple coal reservoirs, western Guizhou region. Front Earth Sci, 15(4): 770–789

Kotarba M J, Rice D D (2001). Composition and origin of coalbed gases in the Lower Silesian Basin, southwest Poland. Appl Geochem, 16(7): 895–910

Lan F, Qin Y, Wang A, Li M, Wang G (2020). The origin of high and variable concentrations of heavy hydrocarbon gases in coal from the Enhong syncline of Yunnan, China. J Nat Gas Sci Eng, 76: 103217

Li G, Qin Y, Shen J, Wu M, Li C, Wei K, Zhu C (2019). Geochemical characteristics of tight sandstone gas and hydrocarbon charging history of Linxing area in Ordos Basin, China. J Petrol Sci Eng, 177: 198–207

Li Q, Ju Y, Bao Y, Li X, Sun Y (2015). Composition, origin, and distribution of coalbed methane in the Huaibei Coalfield, China. Energy Fuels, 29(2): 546–555

Li Q, Ju Y, Bao Y, Yan Z, Li X, Sun Y (2014). Origin types of CBM and their geochemical research progress. J China Coal Soc, 39(5): 806–815

Li Y, Fu H, Yan D, Su X, Wang X, Zhao W, Wang H, Wang G (2022b). Effects of simulated surface freshwater environment on in situ microorganisms and their methanogenesis after tectonic uplift of a deep coal seam. Int J Coal Geol, 257: 104014

Li Y, Pan S, Ning S, Shao L, Jing Z, Wang Z (2022a). Coal measure metallogeny: metallogenic system and implication for resource and environment. Sci China Earth Sci, 65(7): 1211–1228

Li Y, Tang D, Fang Y, Xu H, Meng Y J (2014). Distribution of stable carbon isotope in coalbed methane from the east margin of Ordos Basin. Sci China Earth Sci, 57(8): 1741–1748

Li Y, Zhang C, Tang D, Gan Q, Niu X, Wang K, Shen R (2017). Coal pore size distributions controlled by the coalification process: an experimental study of coals from the Junggar, Ordos, and Qinshui basins in China. Fuel, 206: 352–363

Lin Y (2021). Geological controls and high productivity model of low-rank coalbed methane reservoir in the Huanglong Coalfied, Shaanxi, China. Dissertation for Doctoral Degree. Xuzhou: China University of Mining and Technology

Lin Y, Qin Y, Duan Z, Ma D, Chen L (2021b). *In-situ* stress and permeability causality model of a low-rank coalbed methane reservoir in southwestern Ordos Basin, China. Petrol Sci Technol, 39(7–8): 196–215

Lin Y, Qin Y, Ma D, Duan Z (2021a). Pore structure, adsorptivity and influencing factors of high-volatile bituminous coal rich in inertinite. Fuel, 293: 120418

Lin Y, Qin Y, Ma D, Zhao J (2020). Experimental research on dynamic variation of permeability and porosity of low-rank inert-rich coal under stresses. ACS Omega, 5(43): 28124–28135

Meng Z, Yan J, Li G (2017). Controls on gas content, carbon isotopic abundance of methane in Qinnan-east coalbed methane block, Qinshui Basin, China. Energy Fuels, 31(2): 1502–1511

Milkov A V, Etiope G (2018). Revised genetic diagrams for natural gases based on a global dataset of >20000 samples. Organ Geochem, 125: 109–120

Milkov A V, Faiz M, Etiope G (2020). Geochemistry of shale gases from around the world: composition, origins, isotope reversals and rollovers, and implications for the exploration of shale plays. Organ Geochem, 143: 103997

Moore T A (2012). Coalbed methane: a review. Int J Coal Geol, 101(1): 36–81

Ni Y, Dai J, Zou C, Liao F, Shuai Y, Zhang Y (2013). Geochemical characteristics of biogenic gases in China. Int J Coal Geol, 113: 76–87

Qin S, Tang X, Song Y, Wang H (2006). Distribution and fractionation mechanism of stable carbon isotope of coalbed methane. Sci China Earth Sci, 49(12): 1252–1258

Qin Y, Moore T A, Shen J, Yang Z, Shen Y, Wang G (2018). Resources and geology of coalbed methane in China: a review. Int Geol Rev, 60(5–6): 777–812

Qin Y, Tang X, Ye J, Jiao S (2000). Distribution and genesis of stable carbon isotope of coalbed methane in China. J China Univ Min Technol, 29: 113–119

Rice D D (1993). Composition and origins of coalbed gas. In: Law B E, Rice D D, eds. Hydrocarbons from Coal. AAPG Studies in Geology, 38: 159–184

Rice D D, Claypool G E (1981). Generation, accumulation and resource potential of biogenic gas. AAPG Bull, 65: 5–25

Schoell M (1980). The hydrogen and carbon isotopic composition of methane from natural gases of various origins. Geochim Cosmochim Acta, 44(5): 649–661

Scott A R, Kaiser W R, Ayers J W B (1994). Thermogenic and secondary biogenic gases, San Juan Basin, Colorado and New Mexico–implications for coalbed gas producibility. AAPG Bull, 78: 1186–1209

Smith J W, Pallasser R J (1996). Microbial origin of Australian coalbed methane. AAPG Bull, 80(6): 891–897

Strąpoć D, Schimmelmann A, Mastalerz M (2006). Carbon isotopic fractionation of $CH_4$ and $CO_2$ during canister desorption of coal. Organ Geochem, 37(2): 152–164

Tang Y, Gu F, Wu X, Ye H, Yu Y, Zhong M (2018). Coalbed methane accumulation conditions and enrichment models of Walloon Coal

measure in the Surat Basin, Australia. Nat Gas Indus, 5(3): 235–244

Tao M, Chen X, Li Z, Ma Y, Xie G, Wang Y, Wei L, Wang Z, Tang X (2021). Variation characteristic and mechanism of carbon isotope composition of coalbed methane under different conditions and its tracing significance. Fuel, 302: 121039

Tao S, Chen S, Pan Z (2019). Current status, challenges, and policy suggestions for coalbed methane industry development in China: a review. Energy Sci Eng, 7(4): 1059–1074

Tian W, Shao L, Zhang J, Zhao S, Huo W (2015). Analysis of genetic types of the coal bed methane of Jurassic formation, southern Ordos Basin. China Min Mag, 24: 81–85

Vinson D S, Blair N E, Martini A M, Larter S, Orem W H, Mcintosh J C (2017). Microbial methane from in situ biodegradation of coal and shale: a review and reevaluation of hydrogen and carbon isotope signatures. Chem Geol, 453: 128–145

Wang Q, Xu H, Tang D, Yang S, Wang G, Ren P, Dong W, Guo J (2022). Indication of origin and distribution of coalbed gas from stable isotopes of gas and coproduced water in Fukang area of Junggar Basin, China. AAPG Bull, 106(2): 387–407

Whiticar M J (1996). Stable isotope geochemistry of coals, humic kerogens and related natural gas. Int J Coal Geol, 32(1–4): 191–215

Whiticar M J (1999). Carbon and hydrogen isotope systematic of bacterial formation and oxidation of methane. Chem Geol, 161(1–3): 291–314

Whiticar M J, Faber E, Schoell M (1986). Biogenic methane formation in marine and fresh water environment: $CO_2$ reduction vs. acetate fermentation-isotopic evidence. Geochim Cosmochim Acta, 50(5): 693–709

Xin F, Xu H, Tang D, Cao C (2022). Differences in accumulation patterns of low-rank coalbed methane in China under the control of the first coalification jump. Fuel, 324: 124657

Xing L T, Li Z P, Xu L, Li L W, Liu Y (2022). Application of chromium catalysis technology to compound-specific hydrogen isotope analysis of natural gas samples. Talanta, 239: 123133

Xu H, Tang D, Liu D, Tang S, Yang F, Chen X, He W, Deng C (2012). Study on coalbed methane accumulation characteristics and favorable areas in the Binchang area, southwestern Ordos Basin, China. Int J Coal Geol, 95: 1–11

Zhang J, Zhao J, Chen D, Li S, Lin H (2020). Sedimentary environment characteristics and genesis of $H_2S$-bearing coal seam in Binchang Mining Area, Ordos Basin. Nat Gas Geosci, 31(1): 100–109

Zhang K, Meng Z, Wang X (2019a). Distribution of methane carbon isotope and its significance on CBM accumulation of No. 2 coal seam in Yanchuannan CBM block, Ordos Basin, China. J Petrol Sci Eng, 174: 92–105

Zhang S, Zhang X, Li G, Liu X, Zhang P (2019b). Distribution characteristics and geochemistry mechanisms of carbon isotope of coalbed methane in central-southern Qinshui Basin, China. Fuel, 244: 1–12

Zhao J, Zhang Q, Zheng K, Li C, Chen D (2018). Disaster-causing mechanism of surrounding rock gas flowing underground in the Huangling coal mine and prevention measures. J Nat Gas Indust, 38(11): 114–121

Zhou B, Qin Y, Yang Z (2020). Ion composition of produced water from coalbed methane wells in western Guizhou, China, and associated productivity response. Fuel, 265: 116939